Probing Graphene Edges *via* Raman Scattering

Awnish K. Gupta,[†] Timothy J. Russin,[†] Humberto R. Gutiérrez,[†] and Peter C. Eklund[†,‡,*]

[†]Department of Physics and [‡]Department of Materials Science & Engineering and Materials Research Institute, The Pennsylvania State University, University Park, Pennsylvania 16802

ABSTRACT We present results of a Raman scattering study from the region near the edges of *n*-graphene layer films. We find that a Raman band (D) located near 1344 cm^{-1} (514.5 nm excitation) originates from a region next to the edge with an apparent width of ~70 nm (upper bound). The D-band was found to exhibit five important characteristics: (1) a single Lorentzian component for $n = 1$, and four components for $n = 2-4$, (2) an intensity $I_D \sim \cos^4 \theta$, where θ is the angle between the incident polarization and the average edge direction, (3) a local scattering efficiency (per unit area) comparable to the G-band, (4) dispersive behavior (~50 cm^{-1}/eV for $n = 1$), consistent with the double resonance (DR) scattering mechanism, and (5) a scattering efficiency that is almost independent of the crystallographic orientation of the edge. High-resolution transmission electron microscope images reveal that our cleaved edges exhibit a sawtooth-like roughness of ~3 nm (*i.e.*, ~20 times the C−C bond length). We propose that in the double resonance Raman scattering process the photoelectron scatters diffusely from our edges, obscuring the recently proposed strong variation in the scattering from armchair *versus* zigzag symmetry edges based on theoretical arguments.

KEYWORDS: graphene · *n*-graphene layers · edge Raman scattering · edge structure TEM · polarized Raman scattering

Well before the experimental discovery of graphene,[1,2] the electronic states associated with a graphene edge were the focus of extensive theoretical research.[3−5] Various symmetry edges were predicted to have localized electronic edge states, while others were not.[4,6] Localized edge states affect the physical properties of graphene; for example, they can induce ferromagnetism,[4] superconductivity,[7] and an anomalous quantum Hall effect.[8] Graphene edges with magnetic properties have been proposed as a possible system for use in spintronics,[9,10] and they have recently been observed in graphite *via* scanning tunneling microscopy (STM) experiments.[11,12]

Theory has indicated that a double resonance (DR) Raman scattering process can explain the existence of a high-frequency (~1350 cm^{-1}) Raman band identified with the edge of a hexagonal sp^2 carbon network.[13−16] An edge is a one-dimensional localized defect that theory argues provides the necessary elastic and specular scattering of the photoexcited electrons to produce a zone corner optical phonon in the DR process.[16] It has also been predicted that only an armchair symmetry edge will participate in this DR defect-induced scattering.[13]

In this paper, we present the results of micro-Raman scattering and high-resolution transmission electron microscopy (HRTEM) studies on the edges of micromechanically produced[2] single-layer ($n = 1$) and *n*-layer graphene systems (*n*GLs; $2 \leq n \leq 4$). We also compare our Raman results from the studies of edges of large area films to those recently obtained on 2−3 nm wide GNRs produced by chemical exfoliation.[17] We show that the Raman scattering associated with the edge is sensitive to *n*, polarized along the average direction of the edge and is localized to within ~70 nm of the edge.

RESULTS AND DISCUSSION

The only one-phonon Raman bands that are symmetry-allowed in graphite are those identified with the E_{2g} symmetry zone center phonons; they occur at 42 and 1582 cm^{-1}.[18] The low-frequency E_{2g} mode involves a rigid shearing of one layer relative to the next and therefore involves the stretching of weak interlayer bonds. The high-frequency E_{2g} mode gives rise to the G-band and also involves the stretching of strong intralayer bonds. Two other prominent one-phonon bands can often be observed in disordered graphitic materials. They are referred to as the D- and D′-bands, where D refers to "defect" scattering.[18,19] These usual D-bands are observed near ~1350 cm^{-1} (D) and 1620 cm^{-1} (D′) (514.5 nm excitation). Both D and D′ are dispersive; that is, the Raman band frequency

*Address correspondence to pce3@psu.edu.

Received for review June 12, 2008 and accepted November 18, 2008.

Published online December 15, 2008. 10.1021/nn8003636 CCC: $40.75

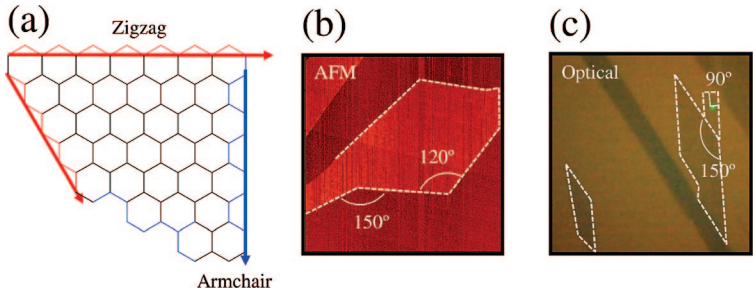

Figure 1. (a) Schematic zigzag and armchair edge structures. (b,c) AFM and optical images, respectively, of micromechanically cleaved edges. Note that these *n*GL films exhibit angles between adjacent edges that are multiples of 30°. In (b) and (c), the dashed lines indicate the average edge position.

changes with excitation laser energy. Recently, we have observed another Raman band at ~1350 cm^{-1} has been observed in bilayer graphene that has been called the "I-band"; this band has been identified with incommensurate stacking disorder or, equivalently, rotational stacking disorder of the two layers (unpublished results).

The dispersive behavior of the D- and D′-bands in sp^2 carbons can be understood within the context of double resonance (DR) Raman scattering.[14,16,20,21] A theoretical framework is in place to help identify the various types of lattice defects that might participate, such as missing C-atoms, heptagon−pentagon pairs, heteroatoms (*e.g.*, boron), a grain boundary, an edge or finite basal plane crystallite effects.[20,22] In general, the DR process involves several steps, including phonon emission and elastic electron scattering to complete the roundtrip Raman transition from and to the electronic ground state. So-called "intervalley" and "intravalley" DR processes are responsible for the D and D′ Raman bands, respectively. Inter- and intravalley scattering in the DR process refers to whether the photoexcited electron scatters between electronic states within the same carrier pocket (intra) or between states in inequivalent carrier pockets (inter) located at the K and K′ points in the Brillouin zone.[15,16] To conserve wavevector in the overall DR scattering process, large wavevector phonons (~zone corner) are produced from intervalley scattering (Raman D-band), and much shorter wavevector phonons are produced from intravalley scattering (Raman D′-band).

In many cases, *n*GL films prepared *via* micromechanical cleavage exhibit an *average* angle between adjacent edges that is a multiple of 30°.[13,23] This angle might be interpreted as evidence for the presence of predominantly smooth zigzag or armchair edges. It is easy to show that an armchair edge adjacent to a zigzag edge will be separated by an angle $\theta = (2p + 1) \times 30°$, and adjacent zigzag edges or armchair edges will be separated by $\theta = 2p \times 30°$, where p is an integer.[18] In Figure 1a, we show schematic examples of armchair and zigzag edges. We also observe edges with multiples of 30° between them, as shown in the AFM image (Figure 1b) and optical image (Figure 1c). For clarity, the average edge direction is represented in these figures by the dashed lines superimposed on the image.

Recent studies of defect-induced Raman scattering from the edges of graphite crystals have been reported by Cancado *et al.*[13] From a theoretical perspective, they argue that intervalley DR scattering and a D-band could occur only from an armchair-type edge. We test these ideas in graphene, where only one layer can contribute to the D-band scattering, rather than all layers within the ~50 nm optical skin depth[24] of their graphite sample. We also examine the D-band scattering from edges of *n*GLs ($n = 2-4$).

Figure 2a shows Raman spectra in the range of ~1200−1700 cm^{-1} collected at room temperature from a graphene ($n = 1$) film supported on a $Si:SiO_2$ substrate when the incident beam was focused near the center of the film (top) or near the edge of the film (bottom). The spectra are offset for clarity. While localized illumination of the center and the edge of the film both produce the usual G-band, edge excitation produces an additional strong D-band at ~1344 cm^{-1} and a very weak D′-band at ~1620 cm^{-1}. In Figure 2b, the spatial distribution of the G-band (integrated intensity) $I_G(x,y)$ is mapped for the entire $n = 1$ sample (note the color scale). The incident and scattered polarizations were chosen parallel to the horizontal direction (top edge of film in Figure 2b). $I_G(x,y)$ can be seen to be essentially constant over the entire film, except near the edges. The D-band integrated intensity $I_D(x,y)$, on the other hand, can be seen in Figure 2c to be localized near the edges of the film. Also noteworthy in Figure 2c is the difference in D-band intensity observed at adjacent edges (*e.g.*, the bottom and left edges), which suggests a polarization dependence. The G-band intensity, on the other hand, exhibits no such polarization dependence for excitation in the central region or near the edges. We discuss the polarization behavior of the

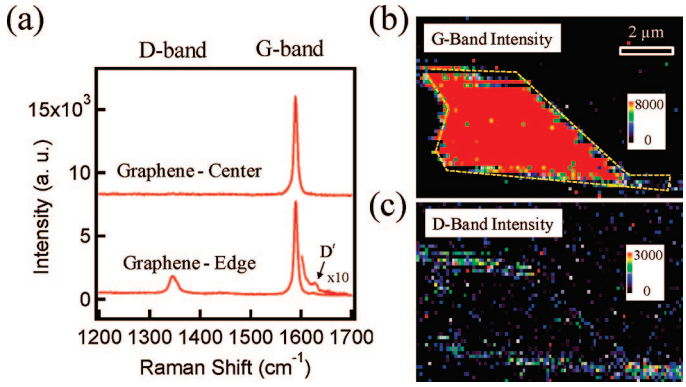

Figure 2. (a) First-order micro-Raman spectra of a $n = 1$ film collected with localized excitation in a micro-Raman instrument: (top spectrum) excitation near the center of the film, (bottom spectrum) excitation near an edge showing the additional presence of D- and D′-bands. (b,c) Integrated intensity maps of the G-band (b) and D-band (c) for the entire $n = 1$ film. Raman spectra were collected at room temperature using 514.5 nm laser excitation. Color scale indicates the intensity in arbitrary units.

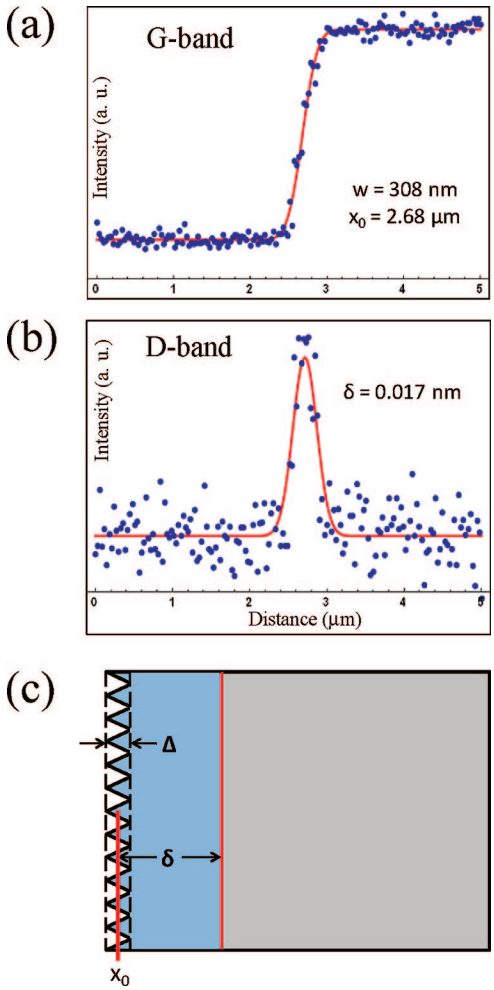

Figure 3. (a) Measured G-band integrated intensity (dots) *versus* focal spot position (x) as the spot is scanned across the edge of the film; solid line is a least-squares fit to the data (eq 2). The fit locates the edge (x_0 = 2.68 ± 0.004 μm) of the film and the excitation beam waist w; for this data set, w = 308 ± 12 nm. (b) Measured D-band integrated intensity (dots) *versus* position; solid line is a least-squares fit to the edge scattering assumed localized to within δ nm of the edge (eq 2); for this particular data set, δ ± 37 nm. (c) Schematic view of an idealized graphene edge with D scattering limited to within a distance δ of the edge that has sawtooth roughness Δ. Spectra collected with 514.5 nm excitation.

D-band and G-band in more detail toward the end of this paper.

In an effort to characterize the spatial extent of the region over which the D-band scattering originates, we translated the laser focal spot across the edge of the film as described in the Experimental Details. We collected the integrated intensity for the G- and D-bands at each point in the scan (spaced Δx = 30 nm apart); the incident and scattered radiation was polarized parallel to the edge. The data for the x dependence of the G- and D-bands are displayed in Figure 3. The G-band intensity (Figure 3a) is seen to rise as the edge is approached and then saturate at a constant value, while the D-band (Figure 3b) is seen to be localized at the edge. The profile of the laser focal spot broadens both the onset of the G-band intensity as well as the spatial width of the D-band. Assuming the G-band intensity is a step function centered at the position of the average edge, we can use the spatial dependence of the G-band intensity to determine the Gaussian parameters of the laser focal spot. Once the focal spot is parametrized, we can attempt to deconvolute the laser spot from the width of the spatial extent of the D-band scattering.

The Raman band intensity profile $I(x,y)$ is given by the two-dimensional convolution integral

$$I(x,y) = \int I_L(x'',y'')S(x-x'',y-y'')\mathrm{d}x''\,\mathrm{d}y'' \quad (1)$$

where I_L and S describe the spatial dependence of the laser intensity and the local Raman scattering efficiency, respectively. The profile of the focal spot is taken to be that of a Gaussian laser beam centered at (x',y') with a waist w[25]

$$I_L(x,y) = I_0 \exp\{-2[(x-x')^2+(y-y')^2]/w^2\} \quad (2)$$

For the G- and D-bands, we assume that $S(x,y)$ will be given by (cf. Figure 3c)

$$S_G = S_{G_0} \text{ for } x > x_0 \text{ and } S_G = 0 \text{ for } x < x_0 \quad (3a)$$

$$S_D = S_{D_0} \text{ for } x_0 < x < x_0 + \delta \text{ and } S_D = 0 \text{ otherwise} \quad (3b)$$

where S_G and S_D can be recognized, respectively, as a step function located at x_0 and a boxcar function starting at x_0 with width δ (Figure 3c). The forms chosen for S_G and S_D are consistent with the assumption of a constant local scattering efficiency per unit area for the G-band from anywhere in the film and a local uniform D-band scattering efficiency within a distance δ from the edge.

Using eqs 2 and 3, we can obtain an analytical function to describe the integrated G-band scattering intensity as a function of the center of the excitation spot relative to the edge located at x_0. We find the expression

$$I_G(x) = \sqrt{\frac{\pi}{8}}Aw\left(1+Erf\left(\frac{\sqrt{2}(x-x_0)}{w}\right)\right) \quad (4)$$

where $Erf(x)$ is the Gaussian error function and the scaling factor is $A = S_G I_0$. Fitting this function to the experimental $I_G(x)$, we can obtain a value for the Gaussian laser beam waist w. The result of a typical fit is shown as the solid line in Figure 3a. The average from fitting 10 different graphene (n = 1) edge data sets, such as shown in Figure 3a, returned the result w = 400 ± 50 nm, where the error is the standard deviation in w over these 10 experiments. This average value for w is in reasonable agreement with advertised values for our microscope objective, but well above the calculated ideal diffraction-limited waist $w_d \sim$ 175 nm.

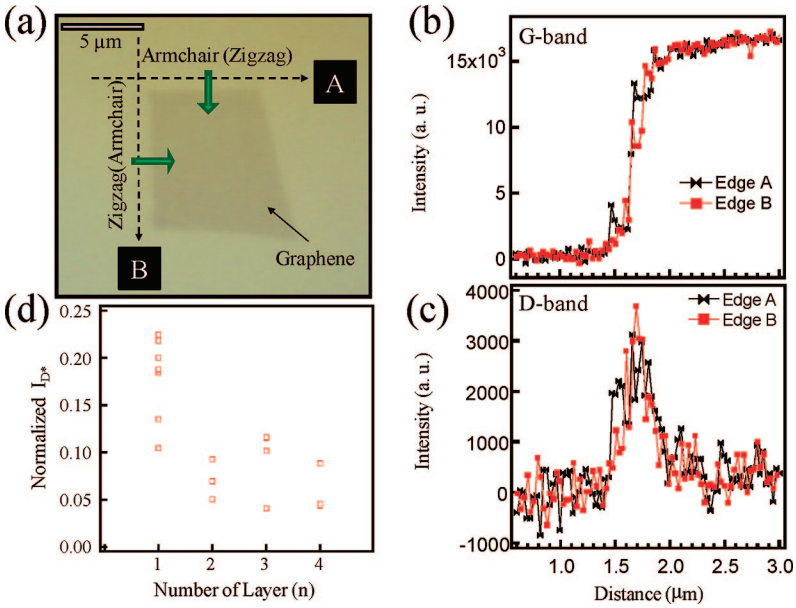

Figure 4. (a) Optical image of a single-layer graphene flake with orthogonal adjacent edges (dashed lines). (b,c) Measured integrated intensity (dots) *versus* position (*x*) for line scans across edges A and B: (b) G-band, (c) D-band. Data are superimposed without scaling. (d) Measured normalized maximum integrated D-band intensity *versus* the number of layers *n* in the film. Micro-Raman spectra were collected with 514.5 nm laser excitation. Incident and scattering light polarizations were kept parallel to the edges. Spectra collected with 514.5 nm excitation.

We also considered the effect of an ideal meandering edge (sawtooth), as shown schematically in Figure 3c. Values for w obtained including the sawtooth complication (peak to notch value $\Delta = 3$ nm is consistent with TEM images of real edges; see below) produced a difference in w of 0.05 nm relative to the value for a straight edge. We therefore ignored this complication in our analysis.

To determine the range over which the D-band scattering occurs, we performed the convolution (eq 2) using the boxcar function (eq 3b) and find

$$I_D(x) = \sqrt{\frac{\pi}{8}} ABw\left(Erf\left(\frac{\sqrt{2}(x - x_0)}{w}\right) + Erf\left(\frac{\sqrt{2}(\delta - x + x_0)}{w}\right)\right) \quad (5)$$

Note that A, w, and x_0 can be determined from the fit to $I_G(x)$. These are substituted in eq 5 before the function is fit to $I_D(x)$ to determine the scale factor B and the width δ. Each D-band was fit using the parameters obtained from the corresponding G-band fit. An example of a fit is shown in Figure 3b and returned $\delta = 0.002 \pm 37$ nm. The large statistical error (36 nm) is due to the scatter of the data for this particular data set. Values for δ obtained by a series of similar least-squares fits ranged over $0 < \delta < 0.05$ nm and with an error σ (*i.e.*, one standard deviation) ranging over $14 < \sigma < 66$ nm. Averaging our fits resulted in $\delta = 0.03$ nm and $\sigma = 36$ nm. Assuming a Gaussian noise distribution, we can say with 95% certainty that the value of δ lies within 2σ of the measured value. Thus, a conservative upper bound for the range from which the D-band scattering can occur is $\delta = 72$ nm.

We next present data that attempt to address whether the D scattering can be identified with only one type of edge (*i.e.*, an armchair edge). Figure 4a shows an optical image of a graphene $n = 1$ film with two adjacent edges (marked "A" and "B" in the figure). The edges are separated by an average angle of 90°, as determined over edge lengths of several microns; this suggests that one edge of the film is zigzag and the other is armchair (see Figure 1a). The essential ideas behind the D (edge) scattering theory are three-fold:[13,20] (1) elastic scattering of the photoexcited electron must occur at the edge, such that the momentum component parallel to the edge is conserved while the momentum component perpendicular to the edge is reversed; (2) the edge must be oriented to scatter the electron from one valley to another; and (3) only an armchair edge is properly oriented to accomplish (2).

To observe the proposed edge selectivity, we performed G and D line scans for edges A and B. In each case, the incident and scattered electric fields were polarized parallel to the respective edge. The data for A and B are shown superimposed in Figure 4b for G scattering and in Figure 4c for D scattering. The overlap of the G data for edges A and B (Figure 4b) indicates the stability of our Raman instrument over the time needed to observe I_D for both edges. Interestingly, although edges A and B make an angle 90° to one another (Figure 4a), the raw I_D data for both edges superimpose very nicely (Figure 4c); that is, for this pair of edges we see no significant difference in the scattering efficiency from one edge to the other. Either the theory for the D-band is incorrect or neither edge has dominant armchair symmetry.

Data from Raman line scan studies on 20 *n*GL film edges ($n = 1-4$, 10 different films) are collected in Figure 4d. The scan direction was always perpendicular to the edge under study, and the incident and scattered light polarizations were always parallel to the edge. Raman line scans produced data similar in form to that shown in Figure 4b,c. For simplicity, however, we determined the maximum value I_D^{max} for each line scan from a fit of $I_D(x)$ to a Gaussian function rather than to the convolution (eq 2). For normalization purposes, the plateau of $I_G(x)$ (*cf.*, Figure 4b) from the same line scan was fitted to a constant to obtain I_G^{avg}. In Figure 4d, we compare the maximum spatial D-band intensity for all the edges on various films. Plotted there is the D intensity normalized to the G-band intensity at the plateau; that is, we plot I_D^{max}/I_G^{avg} *versus* the number of layers n in the various films. This normalization with respect to

the G-band helps to eliminate possible fluctuations in I_D^{max}/I_G^{avg} from variations in the excitation or collection efficiency that might arise between experiments on different films (or edges of the same film). The D-band and G-band scattering should both be approximately proportional to the number of layers n. Any n dependence of the data in Figure 4d would therefore be of interest; we do observe a smaller I_D^{max}/I_G^{avg} for larger n. Based on the scatter of the D data for each n, we are unable to conclude that we have observed D scattering from a predominantly pure zigzag or armchair edge. Recall that we preferentially studied films where adjacent edges presented a relative angle exhibiting a multiple of 30°. The idea was to use this indicator to identify a zigzag or armchair edge. So, if theory is correct and our edges are sufficiently smooth, we expect the normalized D maximum intensity data in Figure 4d would be observed to group around two values: a large value for armchair edges and a small value (near zero) for zigzag edges. Separating the data in Figure 4d into two groups can of course be done, but it might not be very convincing. Factors of four in the D scattering are observed depending on the edge and the number of layers in the film, but the grouping of the data in the figure into strong and weak scattering edges is not apparent. We propose an explanation below for the apparent randomness in the normalized D intensity at fixed n.

Before doing so, we should also emphasize another interesting point from Figure 4d. Note that the maximum intensity of the D-band is comparable to that of the G-band collected at the center of the film (*i.e.*, $I_D^{max} \sim 1/4\ I_G$). This is somewhat surprising, considering that D-band scattering is confined to a narrow strip near the edge (width $\delta \sim 72$ nm (upper bound)), yet the G-band scattering is uniform over the entire film. For the sake of discussion, we *assume* the same scattering efficiency per hexagon for both the D- and G-bands; we can then use the convolution integrals to predict the intensity ratio I_D^{max}/I_G^{avg} for $\delta \sim 72$ nm taking into account the size of the focal spot relative to δ. Using eqs 2 and 3, we calculate $I_D^{max}/I_G^{avg} \sim 0.14$, about a factor of 2 less than measured (see Figure 4d). However, if $\delta \ll 72$ nm (upper bound), the D scattering efficiency per unit area becomes much larger than the G scattering, and this enhancement would require a theoretical explanation *via* the appropriate matrix elements within the context of DR scattering.

In Figure 5, we show HRTEM images of typical graphene edges produced for $n = 1$ graphene by micromechanical cleavage. Figure 5a shows a typical graphene edge under high magnification. Although the edge is, on average, straight over hundreds of nanometers, it exhibits a sawtooth roughness of approximately ~3 nm, which should be compared to the in-plane C−C bond length of $a = 0.142$ nm. In Figure 5b, we display a TEM image of a notch which has adjacent

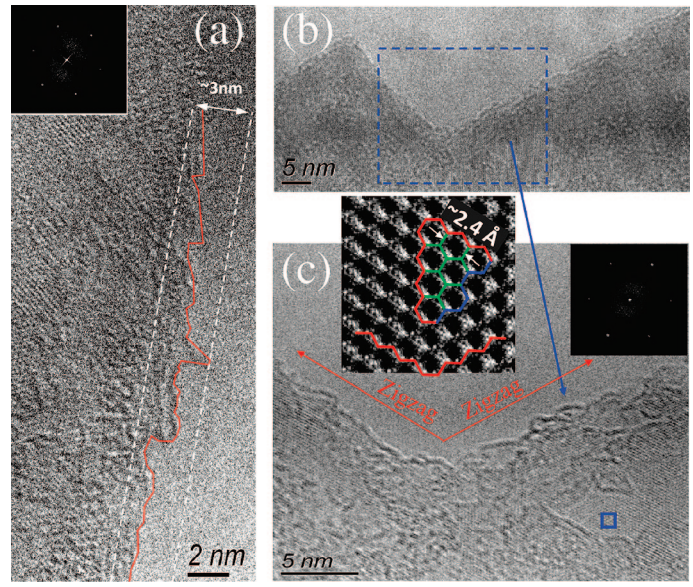

Figure 5. HRTEM images of two different graphene $n = 1$ edges. (a) Red line indicates the position of the edge. Sawtooth roughness Δ of the edge is ~3 nm. (b and c) Image of same notch under different magnification. Insets to (c): (right) diffraction pattern obtained by Fourier transform of entire near-notch region, (left) Fourier-filtered image of the region in the small blue square. The edges near the notch run approximately parallel to zigzag directions.

edges that form an external angle of approximately 120° (*i.e.*, 4 × 30°). One might therefore assume that both edges exhibit zigzag symmetry. In Figure 5c, this same notch is imaged under higher magnification. The sharp spot pattern in Figure 5c (inset, top right) is the Fourier transform (FT) of the exceptionally high-quality image region inside the dashed-lined box in Figure 5b. The FT indicates that the graphene near the notch is a single-crystal domain. We Fourier-filtered the exceptionally high-quality image region (inside the solid-lined box in Figure 5c) to find the orientation of the sp^2 network near the notch. The result is also shown in Figure 5c (inset, top center) and establishes the armchair (blue) and zigzag (red) directions in the film close to the notch. The edges on either side of the notch therefore run parallel (on average) to zigzag edges. However, as shown in the TEM image (Figure 5c), the actual edge exhibits an approximate sawtooth roughness of $\Delta \sim 3$ nm; that is, the edge is a factor of 10−20 rougher than an atomically smooth zigzag edge. For comparison to Δ, we can estimate the wavelength of the photoexcited electrons (λ_e) produced in our experiments. For vertical transitions between linear bands, the simple relationship between photoelectron wavelength and laser photon energy E_p is given by $\lambda_e = 2hv_F/E_p$, where h is Planck's constant, $v_F \sim 10^6$ m/s[26,27] is the Fermi velocity of graphene and $E_p = 2.4$ eV in our experiments. Accordingly, we find $\lambda_e \lesssim 3.4$ nm, which is comparable to the typical edge roughness $\Delta \sim 3$ nm obtained *via* TEM. By analogy to diffuse scattering of photons from optically rough surfaces, we expect diffuse photoelectron scattering when $\lambda_e \lesssim \Delta$. We therefore propose that our

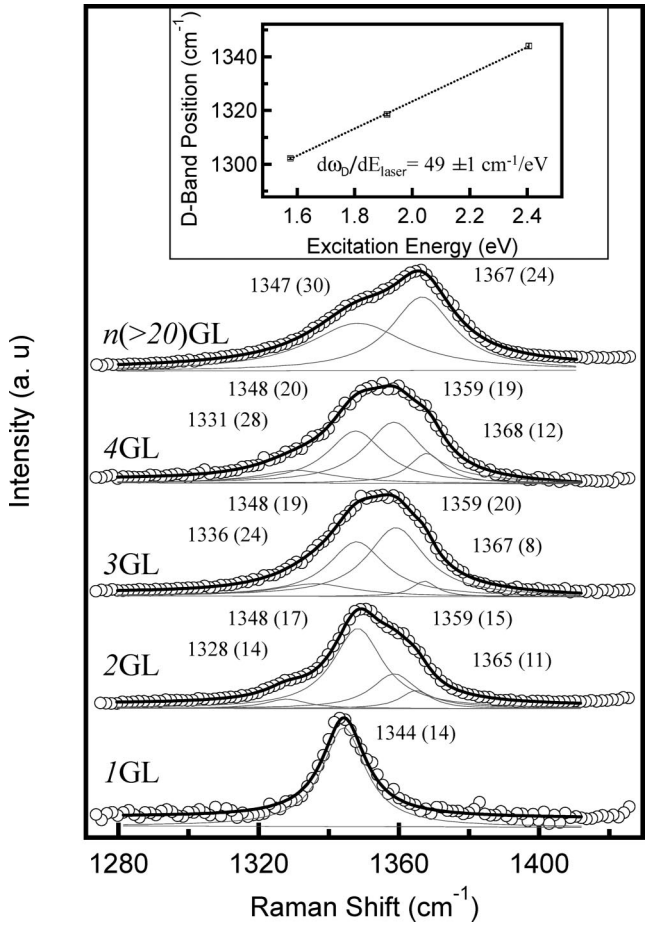

Figure 6. Raman D-bands (edge excitation) for various *n*-layer films. Micro-Raman spectra were collected using a 514.5 nm laser excitation. Incident and scattered light polarization were kept parallel to the *n*GL edges. (Inset) D-band dispersion for graphene; slope is 49 ± 1 cm^{-1}/eV.

graphene edges are too rough to engage in specular scattering of the incident photoelectron, and the proposed selection rule (armchair) for localized D-band scattering for armchair edges breaks down as a result. We observed smaller normalized D-band intensity for higher *n* (Figure 4d). This behavior is consistent with the presence of a smoother edge for higher *n*. As the edges become smoother, D scattering will start to favor selectivity of edge structure *via* specular electron scattering. For this case, we should expect to see strong scattering from armchair edges and weak scattering from zigzag edges. Indeed, the grouping of the data in the figure into strong and weak scattering edges is more pronounced for $n = 3$ and $n = 4$ than $n = 1$ or $n = 2$ data in Figure 4d. This intensity variation for single-layer graphene ($n = 1$) in Figure 4d can be attributed to the different edge roughness for different flakes. This view is also in accord with the previous observation[13] of strong variation in D-band intensity of armchair and zigzag edges in graphite owing to specular scattering mechanism for smooth graphite edges.

Interestingly, Li *et al.*[17] recently reported the preparation of 2−3 nm wide graphene nanoribbons (GNRs) *via* a chemical exfoliation method. The widths of these GNRs are even smaller than the sawtooth roughness Δ we measured by TEM (Figure 5) for graphene edges produced by cleavage. In fact, our recent Raman scattering measurements (unpublished results) on some of these 2−3 nm GNRs reveal no measurable D-band, although both edges of the ribbon were simultaneously exposed to the laser excitation. We therefore are tempted to conclude that some of these chemically produced GNRs possess almost perfect zigzag edges. Critical evaluation of similarly prepared graphene edges in HRTEM or STM should be carried out to examine whether they are smoother than those obtained by micromechanical cleaving.

In Figure 6, we plot D-bands observed by illuminating the edges of *n*GLs ($n = 1-4, \sim 20$). These D-bands are displayed to indicate possible changes of line shape with *n*. All D-bands were normalized to have equal intensity; the spectra have been plotted with an arbitrary vertical offset for clarity. The solid curves are the result of Lorentzian line shape analyses. As can be seen, graphene ($n = 1$) exhibits the most narrow D-band; it can be well fit by a single Lorentzian component at $\sim$1344 cm^{-1} with a full width at half-maximum (fwhm) = 14 cm^{-1}, including $\sim$1 cm^{-1} of instrumental broadening. For $n = 2$, four Lorentzian components were obtained by the fitting procedure. The component frequencies are listed in the figure together with the associated fwhm presented in parentheses. For $n = 3$ and 4, the least-squares fitting of the D-band also indicated four components. They were observed to exhibit almost the same set of frequencies as found for $n = 2$, but with different relative intensities. For the $n > 20$ sample, a convincing fit to four Lorentzian components cannot be made; the D-band, however, can be well fit by a doublet with two broad components. In the inset to Figure 6, we plot the D-band maximum *versus* laser energy for graphene ($n = 1$). The data were collected with 514.5, 647.1, and 785.0 nm laser excitations. As can be seen, the Raman band dispersion is linear and equal to 49 ± 1 cm^{-1}/eV, which is similar to the dispersion published previously for D-bands in graphite and highly disordered sp^2 carbons[20] and also the D-band (edge) in graphite.[13] Four components for $n = 2$ would be consistent with the DR mechanism, as four different q-vector phonons can participate in intervalley scattering when two pairs of electronic subbands are involved. For $n = 3$ and 4, a four-component D-band suggests that the subband splittings near the electronic wavevector *k* for the initial and final electronic states produce two groups of subbands. Within a group, there is either only one band or the partners are weakly split so as *not* to produce more than four recognizable D-band components.

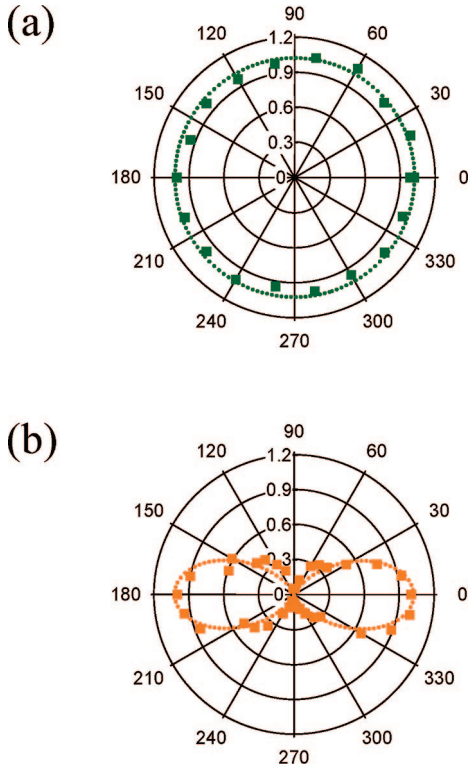

Figure 7. Polar plots of the experimental G- and D-band scattering intensity *versus* polarization angle θ measured relative to the edge of an *n* = *1* film. Incident and scattered radiation were polarized parallel to each other. (a) G-band; excitation localized at the center of the film. The dotted line represents a least-squares fit of a circle to the data (squares). (b) D-band; excitation localized over an edge. The dotted line represents a least-squares fit of the data (squares) to ~cos^4 θ. The fit improves if a small constant term ρ_o is included in the fitting.[28]

In Figure 7, we show polar plots of the Raman scattering intensity *I versus* the angle θ of the incident electric field relative to a nearby edge; the analyzer was also set to collect scattered photons polarized parallel to the incident photons. The G-band data were taken with the laser focal spot sufficiently far from the edge. The dotted circle represents the least-squares fit to the polarized Raman data. The G-band is therefore isotropic (unpolarized), as expected, and shows that there is no instrument function distorting the polarization data.

Even for excitation of the G-band localized at the edge (not shown), the polar plot is nearly circular. The polar plot for the D-band, on the other hand, exhibits strong polarization effects. The D polar data (Figure 7b) can be fit to a cos^4(θ) function (dotted line), suggesting that the D scattering is the result of a product of two cos^2(θ) factors, one for photon absorption and the other for photon emission. The fit is improved by including a constant angle-independent term which allows for a possible experimental error in setting the polarizer parallel to the edge.[28] Possibly the most interesting point about the D polarization is that θ = 0° (*i.e.*, the polarization direction for maximum scattering intensity) always seems to align along the *average* edge direction; this occurs even though HRTEM images (Figure 5) reveal the sawtooth structure of the edge with a roughness 20× that of a C−C bond length. This is an experimental observation for which we have no theoretical explanation at this point in time.

In summary, we have used Raman scattering to study the edges of micromechanically prepared *n*GL films. We find that the D scattering from an edge is confined to a narrow region within δ ~70 nm of the edge, which represents an experimental upper bound; the value for δ could be smaller. Whereas a graphene edge (*n* = 1) produces a narrow single-component defect band, multiple layer films (*n* = 2−4) produce multicomponent D Raman bands. Both these observations and the D-band dispersion are consistent with the DR scattering mechanism. We find that the strength of the D-band scattering is remarkably similar from edge to edge. This suggests that the edge is diffusely scattering the photoexcited electrons in the DR process and obscuring armchair edge selectivity. In fact, the photoelectron wavelength is about the same as the edge roughness. Finally, it is interesting that 1 μm long and 2 nm wide graphene nanoribbons (GNRs) produced via chemical exfoliation were found in our previous Raman study to exhibit a G-band and, in some cases, no D-band. This suggests that chemical exfoliation may produce a much smoother edge than we have been able to prepare by micromechanical cleavage.

EXPERIMENTAL DETAILS

Graphene (*n* = 1) and *n*GL (*n* = 2−4) samples were prepared by micromechanical cleavage[2] of highly oriented pyrolitic graphite (HOPG). The cleaving process occurred either while transferring a thin film from HOPG (438HP-AB, SPI, Inc.) onto Scotch tape (3M, Inc.) or afterward, when rubbing the tape against the substrate. The substrate used in this study was (100)-oriented Si with a 100 nm thermal oxide. Optical microscopy and atomic force microscopy (AFM) were used to identify *n*GLs exhibiting angles between adjacent edges that are multiples of 30° and therefore suggest a "pure" zigzag or armchair structure along the edge.[18]

Polarized Raman scattering measurements were performed with a micro-Raman spectrometer (inVia, Renishaw, Inc.) in the backscattering geometry using a 100× objective lens with N.A. = 0.94. The excitation source was the 514.5 nm line of an argon ion laser (Innova, Coherent, Inc.). Data were collected as a function of position relative to the edge by scanning the laser spot in a line across, and perpendicular to, the edge with a step size of ~30−50 nm. Scattering intensity was also measured as a function of polarization using a rotatable half-wave plate. *n*GL samples for transmission electron microscopy (TEM) were prepared on a SiN-TEM grid (SPI, Inc. part no. 4109SN-BA) with 3 μm diameter holes in a 500 nm thick SiN membrane. *n*GL flakes were deposited on the grid as described earlier by rubbing the Scotch tape (with *n*GLs) across the TEM grid.

The number of layers (*n*) in a *n*GL was determined using Raman spectroscopy.[29−31] Films with *n* = 1 are highly transparent. The value of *n* can be confirmed by observing the "2D" Raman band at ~2680 cm^{-1} (514.5 nm excitation), which is quite

narrow (~25 cm^{-1}) and well fit by a single Lorentzian peak. For $n > 1$, the films become progressively darker; the 2D band contains multiple peaks and is much wider. Therefore, the procedure we use to determine n was initiated by locating an $n = 1$ flake *via* the 2D Raman band. Higher n films ($n = 2, 3,...$) were identified by their G-band (~1580 cm^{-1}) intensity measured relative to that obtained for a $n = 1$ film. For $n < \sim 10$, the G-band intensity increases linearly with increasing n.[30,31]

Note: We became aware of similar work[32] on graphene edges from Cançado *et al.* during the preparation of this manuscript. They measured the spatial dependence of the D-band to be ~40 nm, which is in good agreement with the upper bound of ~70 nm determined in this work. A detailed comparative discussion between the two works can be found in Supporting Information.

Acknowledgment. The work was supported by the NSF NIRT program DMR ECS0609243. We acknowledge helpful discussions with Dr. P. Lammert and Prof. V. H. Crespi also at Penn State University.

Supporting Information Available: A detailed comparative discussion of Cançado *et al.* This material is available free of charge *via* the Internet at http://pubs.acs.org.

REFERENCES AND NOTES

1. Novoselov, K. S.; Geim, A. K.; Morozov, S. V.; Jiang, D.; Zhang, Y.; Dubonos, S. V.; Grigorieva, I. V.; Firsov, A. A. Electric Field Effect in Atomically Thin Carbon Films. *Science* **2004**, *306*, 666–669.
2. Novoselov, K. S.; Jiang, D.; Schedin, F.; Booth, T. J.; Khotkevich, V. V.; Morozov, S. V.; Geim, A. K. Two-Dimensional Atomic Crystals. *Proc. Natl. Acad. Sci. U.S.A.* **2005**, *102*, 10451–10453.
3. Harigaya, K. The Mechanism of Magnetism in Stacked Nanographite: Theoretical Study. *J. Phys.: Condens. Mater.* **2001**, *13*, 1295–1302.
4. Nakada, K.; Fujita, M.; Dresselhaus, G.; Dresselhaus, M. S. Edge State in Graphene Ribbons: Nanometer Size Effect and Edge Shape Dependence. *Phys. Rev. B* **1996**, *54*, 17954–17961.
5. Wakabayashi, K.; Fujita, M.; Ajiki, H.; Sigrist, M. Electronic and Magnetic Properties of Nanographite Ribbons. *Phys. Rev. B* **1999**, *59*, 8271–8282.
6. Sasaki, K.; Sato, K.; Saito, R.; Jiang, J. Local Density of States at Zigzag Edges of Carbon Nanotubes and Graphene. *Phys. Rev. B* **2007**, *75*, 235430-1–235430-7.
7. Sasaki, K.; Jiang, J.; Saito, R.; Onari, S.; Tanaka, Y. Theory of Superconductivity of Carbon Nanotubes and Graphene. *J. Phys. Soc. Jpn.* **2007**, *76*, 033702-1–033702-4.
8. Abanin, D. A.; Lee, P. A.; Levitov, L. S. Charge and Spin Transport at the Quantum Hall Edge of Graphene. *Solid State Commun.* **2007**, *143*, 77–85.
9. Wang, W. L.; Meng, S.; Kaxiras, E. Graphene Nanoflakes with Large Spin. *Nano Lett.* **2008**, *8*, 241–245.
10. Yazyev, O. V.; Katsnelson, M. I. Magnetic Correlations at Graphene Edges: Basis for Novel Spintronics Devices. *Phys. Rev. Lett.* **2008**, *1*, 047209-1–047209-4.
11. Kobayashi, Y.; Fukui, K.; Enoki, T.; Kusakabe, K.; Kaburagi, Y. Observation of Zigzag and Armchair Edges of Graphite Using Scanning Tunneling Microscopy and Spectroscopy. *Phys. Rev. B* **2005**, *71*, 193406-1–193406-4.
12. Kobayashi, Y.; Kusakabe, K.; Fukui, K.; Enoki, T. STM/STS Observation of Peculiar Electronic States at Graphite Edges. *Physica E* **2006**, *34*, 678–681.
13. Cancado, L. G.; Pimenta, M. A.; Neves, B. R. A.; Dantas, M. S. S.; Jorio, A. Influence of the Atomic Structure on the Raman Spectra of Graphite Edges. *Phys. Rev. Lett.* **2004**, *93*, 247401-1–247401-4.
14. Ferrari, A. C.; Robertson, J. Interpretation of Raman Spectra of Disordered and Amorphous Carbon. *Phys. Rev. B* **2000**, *61*, 14095–14107.
15. Saito, R.; Grueneis, A.; Cancado, L. G.; Pimenta, M. A.; Jorio, A.; Souza Filho, A. G.; Dresselhaus, G.; Dresselhaus, M. S. D-Band Raman Spectra of Graphite and Single Wall Carbon Nanotubes. *Mater. Res. Soc. Symp. Proc.* **2002**, *706*, 277–282.
16. Thomsen, C.; Reich, S. Double Resonant Raman Scattering in Graphite. *Phys. Rev. Lett.* **2000**, *85*, 5214–5217.
17. Li, X.; Wang, X.; Zhang, L.; Lee, S.; Dai, H. Chemically Derived, Ultra-Smooth Graphene Nano-Ribbons for Nanoelectronics. *Science* **2008**, *319*, 1229–1232.
18. Dresselhaus, M. S.; Dresselhaus, G.; Eklund, P. C. *Science of Fullerenes and Carbon Nanotubes*, 1st ed.; Academic Press: New York, 1996.
19. Tuinstra, F.; Koenig, J. L. Raman Spectrum of Graphite. *J. Chem. Phys.* **1970**, *53*, 1126–1130.
20. Pimenta, M. A.; Dresselhaus, G.; Dresselhaus, M. S.; Cancado, L. G.; Jorio, A.; Saito, R. Studying Disorder in Graphite-Based Systems by Raman Spectroscopy. *Phys. Chem. Chem. Phys.* **2007**, *9*, 1276–1291.
21. Saito, R.; Jorio, A.; Souza Filho, A. G.; Grueneis, A.; Pimenta, M. A.; Dresselhaus, G.; Dresselhaus, M. S. Dispersive Raman Spectra Observed in Graphite and Single Wall Carbon Nanotubes. *Physica B* **2002**, *323*, 100–106.
22. Sato, K.; Saito, R.; Oyama, Y.; Jiang, J.; Cancado, L. G.; Pimenta, M. A.; Jorio, A.; Samsonidze, G. G.; Dresselhaus, G.; Dresselhaus, M. S. D-Band Raman Intensity of Graphitic Materials as a Function of Laser Energy and Crystallite Size. *Chem. Phys. Lett.* **2006**, *427*, 117–121.
23. Banerjee, S.; Sardar, M.; Gayathri, N.; Tyagi, A. K.; Raj, B. Enhanced Conductivity in Graphene Layers and at Their Edges. *Appl. Phys. Lett.* **2006**, *88*, 062111-1–062111-3.
24. Liu, J.; Hou, M. D.; Trautmann, C.; Neumann, R.; Muller, C.; Wang, Z. G.; Zhang, Q. X.; Sun, Y. M.; Jin, Y. F.; Liu, H. W.; Gao, H. J. STM and Raman Spectroscopic Study of Graphite Irradiated by Heavy Ions. *Nucl. Instr. Methods Phys. Res. B* **2003**, *212*, 303–307.
25. Siegman, A. E. *Lasers*, 1st ed.; University Science Books: Sausalito, CA, 1986.
26. Novoselov, K. S.; Geim, A. K.; Morozov, S. V.; Jiang, D.; Katsnelson, M. I.; Grigorieva, I. V.; Dubonos, S. V.; Firsov, A. A. Two-Dimensional Gas of Massless Dirac Fermions in Graphene. *Nature* **2005**, *438*, 197–200.
27. Zhang, Y. B.; Tan, Y. W.; Stormer, H. L.; Kim, P. Experimental Observation of the Quantum Hall Effect and Berry's Phase in Graphene. *Nature* **2005**, *438*, 201–204.
28. The fit improves slightly if, instead of fitting $I_1(\theta) = A_0 \cos^4(\theta)$, we use $I_2(\theta) = \rho_0 + A_1 \cos^4(\theta)$. Here, the important parameter is ρ_0/A_1, which for our fit is 0.12. We propose that this constant term is due to the nonuniformity of the edge.
29. Ferrari, A. C.; Meyer, J. C.; Scardaci, V.; Casiraghi, C.; Lazzeri, M.; Mauri, F.; Piscanec, S.; Jiang, D.; Novoselov, K. S.; Roth, S.; *et al.* Raman Spectrum of Graphene and Graphene Layers. *Phys. Rev. Lett.* **2006**, *97*, 187401-1–187401-4.
30. Graf, D.; Molitor, F.; Ensslin, K.; Stampfer, C.; Jungen, A.; Hierold, C.; Wirtz, L. Spatially Resolved Raman Spectroscopy of Single- and Few-Layer Graphene. *Nano Lett.* **2007**, *7*, 238–242.
31. Gupta, A.; Chen, G.; Joshi, P.; Tadigadapa, S.; Eklund, P. C. Raman Scattering from High-Frequency Phonons in Supported *n*-Graphene Layer Films. *Nano Lett.* **2006**, *6*, 2667–2673.
32. Cancado, L. G.; Beams, R.; Novotny, L. *Optical Measurement of the Phase-Breaking Length in Graphene*; arXiv:0802.3709v1, arXiv.org e-print archive; http://lanl.arxiv.org/PS_cache/arxiv/pdf/0802/0802.3709v1.pdf, **2008**.